



# Intermittency in free vibration of a cylinder beyond the laminar regime

Navrose<sup>1</sup> and Sanjay Mittal<sup>1,†</sup>

<sup>1</sup>Department of Aerospace Engineering, Indian Institute of Technology Kanpur, Kanpur 208 016, India

(Received 31 December 2018; revised 7 April 2019; accepted 12 April 2019; first published online 15 May 2019)

Vortex-induced vibration of a circular cylinder that is free to move in the transverse ( $Y$ ) and streamwise ( $X$ ) directions is investigated at subcritical Reynolds numbers ( $1500 \lesssim Re \lesssim 9000$ ) via three-dimensional (3-D) numerical simulations. The mass ratio of the system for all the simulations is  $m^* = 10$ . It is observed that while some of the characteristics associated with the  $XY$ -oscillation are similar to those of the  $Y$ -only oscillation (in line with the observations made by Jauvtis & Williamson (*J. Fluid Mech.*, vol. 509, 2004, pp. 23–62)), notable differences exist between the two systems with respect to the transition between the branches of the cylinder response in the lock-in regime. The flow regime between the initial and lower branch is characterized by intermittent switching in the cylinder response, aerodynamic coefficients and modes of vortex shedding. Similar to the regime of laminar flow, the system exhibits a hysteretic response near the lower- and higher- $Re$  end of the lock-in regime. The frequency spectrum of time history of the cylinder response shows that the most dominant frequency in the streamwise oscillation on the initial branch is the same as that of the transverse oscillation.

**Key words:** flow–structure interactions, vortex shedding, wakes

## 1. Introduction

Vortex shedding in the wake of an elastically mounted bluff body may result in its vibration. This phenomenon is referred to as vortex-induced vibration (VIV). A circular cylinder is typically used as a canonical shape for the bluff body in most VIV studies. More often than not, the elastic support is modelled as a linear spring and the cylinder is constrained to move in the transverse direction only (henceforth referred to as  $Y$ -only oscillation). For a comprehensive review on the various aspects of VIV, the interested reader is referred to articles by Sarpkaya (2004), Williamson & Govardhan (2004) and Bearman (2011).

<sup>†</sup> Email address for correspondence: [smittal@iitk.ac.in](mailto:smittal@iitk.ac.in)

The response of the fluid–structure system during VIV depends on several flow and structural parameters that are usually expressed in non-dimensional form: for example, Reynolds number, mass ratio and reduced speed. The Reynolds number ( $Re$ ) is based on the free-stream speed ( $U$ ) and diameter of the circular cylinder ( $D$ ). The mass ratio ( $m^*$ ) is the ratio between the mass of the oscillating structure and the mass of the fluid displaced by it. The reduced speed ( $U^*$ ) is defined as  $U/f_n D$ , where  $f_n$  is the natural frequency of the oscillator. If the natural frequency of the structure is close to the vortex shedding frequency then synchronization/lock-in/resonance can occur in the fluid–structure system, wherein the structure experiences a relatively large amplitude of oscillation (Khalak & Williamson 1999). Typically, lock-in occurs over a range of  $U^*$ . Outside this range, the fluid and structure are desynchronized. For moderate mass-ratio systems and at low  $Re$ , the response curve within the lock-in has two branches: the initial and the lower (Singh & Mittal 2005). In the large- $Re$  regime, an additional branch called the upper branch is observed (Khalak & Williamson 1999; Govardhan & Williamson 2000; Navrose & Mittal 2013; Zhao *et al.* 2014). The peak amplitude of transverse oscillation in the large- $Re$  regime is higher than that in the low- $Re$  regime (Williamson & Govardhan 2004). With a decrease in  $m^*$ , the width of the lock-in regime increases, and below a critical  $m^*$  the regime of synchronization extends to infinite reduced speed (Govardhan & Williamson 2002; Ryan, Thompson & Hourigan 2005; Navrose & Mittal 2017).

Compared to  $Y$ -only oscillation, the VIV set-up where the cylinder is free to oscillate in both streamwise and transverse directions ( $XY$ -oscillation) has been relatively less explored, especially beyond the laminar flow regime. Jauvtis & Williamson (2004) carried out experiments with  $XY$ -oscillation for different values of  $m^*$ . The natural frequencies of the oscillator in the transverse and streamwise directions in their work were kept the same. They observed that for  $m^* \gtrsim 6.0$ ,  $Y$ -only and  $XY$ -oscillation are similar in terms of the number of response branches, peak amplitude of transverse oscillation and vortex shedding modes. In the present work, we investigate the transition between the various branches of the cylinder response and desynchronization regimes for a cylinder undergoing  $XY$ -oscillation. The results are compared to those from earlier studies for  $Y$ -only oscillation to bring out the effect of  $XY$ -oscillation over the  $Y$ -only vibration in modifying the transition.

## 2. Problem description, numerical details and mesh convergence

The flow is modelled using the incompressible Navier–Stokes equations in primitive variable form. The cylinder is mounted on an elastic support that is modelled by two identical springs, one each in the streamwise ( $X$ ) and transverse ( $Y$ ) directions. To encourage large-amplitude oscillation, the structural damping coefficient is set to zero. The details of the equations as well as their finite-element formulation can be found in the article by Prasanth & Mittal (2008). The oscillator has been designed such that  $Re$  varies linearly with the reduced speed as  $Re = 678U^*$ . This approach is akin to that usually employed in experiments and has been used for low- $Re$  VIV computations (Prasanth & Mittal 2008; Navrose *et al.* 2014). The design of the oscillator ensures that the peak amplitude of cylinder oscillation in the transverse direction occurs for similar combinations of  $Re$  and  $U^*$  as in the experiments by Govardhan & Williamson (2006). The span of the cylinder is  $4D$ . The mass ratio for all the simulations is  $m^* = 10.0$ .

The computational domain and finite-element mesh are the same as that in our earlier work (Navrose & Mittal 2013). The cylinder spans the entire extent of the

Mesh	Nodes	Elements	$\frac{X_{rms}}{D}$	$\frac{Y_{rms}}{D}$	$\bar{X}/D$	$C_{D_{rms}}$	$C_{L_{rms}}$	$\bar{C}_D$
<i>M1</i>	2 169 234	2 098 600	0.0046	0.3577	0.1694	0.0483	0.1021	1.0508
<i>M2</i>	5 089 693	10 033 000	0.0046	0.3686	0.1686	0.0530	0.1076	1.0420

TABLE 1.  $U^* = 10$  ( $Re = 6780$ ) flow past a freely vibrating cylinder: mesh convergence study.

hexahedral computational domain along the  $z$ -axis. The upstream and downstream boundaries are located at  $10D$  and  $25.5D$ , respectively, from the axis of the cylinder and the blockage is 5%. The adequacy of the extent of the domain was demonstrated by Prasanth & Mittal (2008). The 3-D finite element mesh is generated by stacking 51 slices of a two-dimensional (2-D) mesh along the span. A special mesh moving scheme is utilized to account for the motion of the cylinder. The mesh near the cylinder moves along with it like a rigid body, while the outer boundary remains fixed (Prasanth & Mittal 2008; Navrose & Mittal 2013, 2017).

A no-slip condition is applied to the velocity on the surface of the cylinder. Free-stream values are assigned for the velocity at the upstream boundary. The stress vector is set to zero at the downstream boundary. On the other boundaries, the normal component of the velocity and tangential component of the stress vector in the two directions are prescribed a zero value. The location of the cylinder, its velocity and the boundary conditions are updated at each nonlinear iteration of the time marching solution process.

Details of the mesh-*M1* used for the computations are listed in table 1. A finer mesh (*M2*) is used to check the adequacy of the spatial resolution of mesh *M1*. The test is carried out for  $U^* = 10.0$  ( $Re = 6780$ ). Table 1 summarizes the response of the cylinder and aerodynamic coefficients obtained with the two meshes. The solutions from the two meshes are in good agreement and confirm the adequacy of mesh *M1*.

### 3. Results

#### 3.1. Overview of cylinder response

Figure 1(a) shows the variation of peak amplitude of transverse oscillation of the cylinder ( $A_y^*$ ) with  $U^*$  (and  $Re$ ). In the regime where intermittency is observed between two states,  $A_y^*$  for each state is obtained separately by segregating the time history corresponding to the respective states. Hence, for each  $U^*$  within the intermittent regime, two data points are shown in figure 1(a). It is observed that the fluid–structure system is in the state of lock-in/synchronization for  $4.0 \leq U^* \leq 10.4$  ( $2700 \lesssim Re \lesssim 7050$ ), wherein the cylinder exhibits a relatively large amplitude of oscillation. The regime of desynchronization in terms of  $U^*$ , prior to and beyond the lock-in regime, is denoted respectively by *DS(I)* and *DS(II)* in the figure. Within the lock-in region, three regimes are identified: initial excitation branch (*IB*), intermittent regime and lower branch (*LB*). The two branches – *IB* and *LB* are named based on the similarity of the transverse cylinder response in the present work and earlier  $Y$ -only vibration studies (Khalak & Williamson 1999; Govardhan & Williamson 2000; Williamson & Govardhan 2004; Zhao *et al.* 2014).

Khalak & Williamson (1999), in their experiments, observed that the fluid–structure system exhibits a hysteretic response near the lower- $U^*$  end of the lock-in regime:

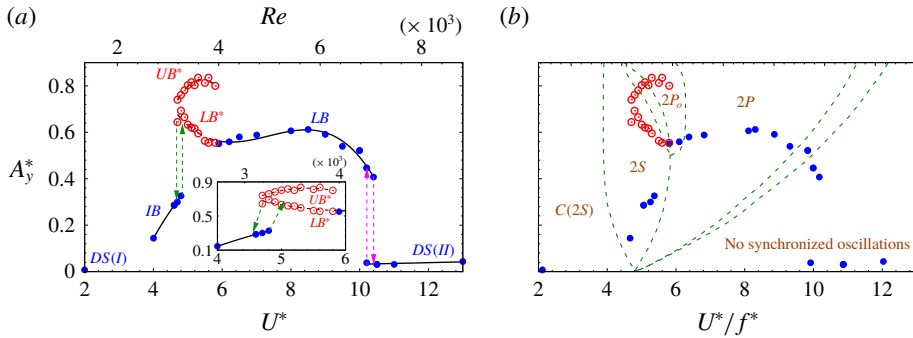


FIGURE 1. Flow past a freely vibrating cylinder: (a) variation of the amplitude of the cylinder oscillation in the transverse direction with  $U^*$  (and  $Re$ ) and (b) superimposition of free-vibration data on the map of vortex shedding regimes derived by Williamson & Roshko (1988). The data points in the regime of intermittency are shown using hollow (red) circles. Other data points are shown via filled (blue) circles. The different branches of the cylinder response, intermittent states and desynchronization regimes are marked in (a). The broken lines, with arrow heads, show hysteresis in the cylinder response with respect to increasing and decreasing  $U^*$ . The inset of (a) shows a close-up view of the cylinder response near the transition between  $IB$  and the intermittent regime.

$A_y^*$  obtained via the increasing- $U^*$  approach in the hysteretic regime is lower than that obtained via the decreasing- $U^*$  approach. In the increasing- $U^*$  approach,  $U^*$  was increased in small increments starting from regime  $DS(I)$  up to regime  $DS(II)$ . In the decreasing- $U^*$  approach,  $U^*$  was decreased in small decrements starting from regime  $DS(II)$  up to  $DS(I)$ . We have adopted the same two approaches in the present work. In the increasing (decreasing)- $U^*$  approach, the increment (decrement) in  $U^*$  is carried out by using the fully developed solution for lower (higher)  $U^*$  as the initial condition for the next reduced speed. After the initial transient stage, the simulation for each  $U^*$  is run for at least 100 cycles of cylinder oscillation in the transverse direction. It is observed that with the increasing- $U^*$  approach, the response of the system first shifts from  $DS(I)$  to  $IB$ , and then jumps at  $U^* = 4.9$  to intermittent switching between high- ( $UB^*$ ) and low-amplitude state ( $LB^*$ ) in the transverse response of the cylinder (see the inset of figure 1a). The asterisk is used in the names to distinguish them from the upper branch ( $UB$ ) and lower branch ( $LB$ ) response reported in experiments (Khalak & Williamson 1999; Govardhan & Williamson 2000; Williamson & Govardhan 2004). The  $UB$  and  $LB$  response, as observed in experiments, can exist either in isolation, or there can be intermittent switching between the two. The  $UB^*$  and  $LB^*$  response, on the other hand, exist only via intermittent switching between the two. The experiments show that the response first jumps from  $IB$  to the upper branch ( $UB$ ), and is followed by intermittent switching between  $UB$  and  $LB$  at a later  $U^*$  (Khalak & Williamson 1999; Govardhan & Williamson 2000; Williamson & Govardhan 2004). We attribute this difference between computational and experimental results to the fact that experiments have been carried out for  $Y$ -only oscillation, while in the present study, the cylinder is free to undergo both transverse and streamwise oscillations. The intermittent behaviour in  $XY$ -oscillation is observed up to  $U^* = 5.8$  (inset of figure 1a). Thereafter, only the  $LB$  response is observed up to  $U^* = 10.4$ , and beyond that the response jumps to  $DS(II)$ . The peak amplitude of cylinder oscillation occurs within the intermittent regime at  $U^* = 5.3$ . The peak value is in good agreement with experimental results of  $Y$ -only oscillation for low- $m^*\zeta$  and a similar range of  $Re$  (Govardhan & Williamson 2000, 2006).

## Intermittency in free vibration at subcritical $Re$

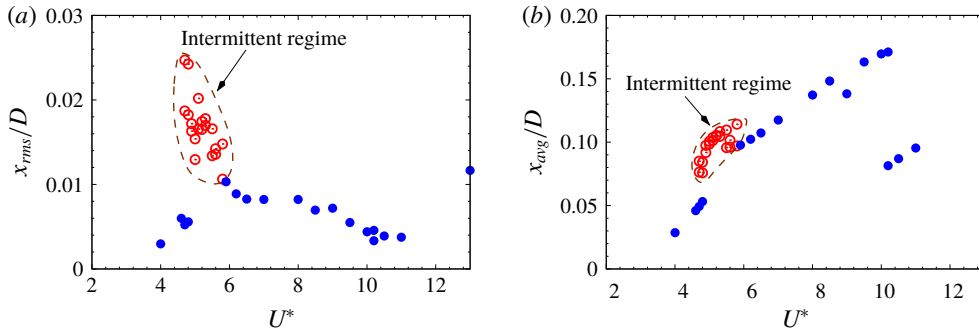


FIGURE 2. Flow past a freely vibrating cylinder: variation of (a) the root mean square of the streamwise oscillation and (b) the time-averaged streamwise location with reduced speed. The data points for the intermittent regime are shown using hollow (red) circles, and are enclosed within a broken closed curve in the two plots.

With the decreasing- $U^*$  approach, hysteresis is observed in the cylinder response near the higher- $U^*$  end of the lock-in regime; the jump from  $DS(II)$  to  $LB$  occurs at  $U^* = 10.2$ , in contrast to the jump from  $LB$  to  $DS(II)$  which takes place at  $U^* = 10.4$ . A hysteretic response is also observed near the lower- $U^*$  end of the lock-in regime, where the intermittent switching between  $UB^*$  and  $LB^*$  with the decreasing- $U^*$  approach extends up to  $U^* = 4.7$ . Singh & Mittal (2005) showed that in the laminar flow regime, the hysteretic response occurs near both the ends of the lock-in regime. It can, therefore, be concluded that the hysteretic response at the two ends of the lock-in regime in free vibration of a circular cylinder is common to both the low- and subcritical- $Re$  flow regimes. Following the nomenclature used for the low- $Re$  flow regime, we refer to hysteresis near the lower- and higher- $U^*$  end of the lock-in regime as primary and secondary hysteresis, respectively. The widths of the primary and secondary hystereses in the present work are found to be the same and are equal to  $\Delta U^* = 0.2$ . This is larger than the corresponding widths reported in the laminar regime (Singh & Mittal 2005). Below  $U^* = 4.7$ , the response moves to  $IB$ , and with further decrease in  $U^*$ , the fluid-structure system reaches a desynchronized state.

Figure 1(a) brings out an interesting feature of free vibration that is possibly being reported for the first time. For  $4.7 \leq U^* \leq 4.9$ , the response may belong to either  $IB$  or intermittently switch between high- and low-amplitude states. With the increasing- $U^*$  approach, the response belongs to  $IB$ , while it switches intermittently between  $UB^*$  and  $LB^*$  for the decreasing- $U^*$  approach. Figure 2(a) shows the variation of the root mean square (r.m.s.) of the streamwise displacement with  $U^*$ . The streamwise fluctuation within the lock-in regime is found to be higher than in the desynchronization regime. The peak r.m.s. value is nearly three times that in the laminar flow regime (Singh & Mittal 2005). Further, unlike the laminar regime, where the peak r.m.s. value occurs near the higher- $U^*$  end of the lock-in regime, it occurs in the intermittent regime towards the lower- $U^*$  end of the lock-in regime for subcritical- $Re$ . The time-averaged streamwise displacement (figure 2b) increases with  $U^*$  in the lock-in regime, with a discernible jump near the two ends of the intermittent regime.

### 3.2. Initial branch: $4.0 \leq U^* \leq 4.9$

Figure 3 shows the time histories of cylinder displacement and aerodynamic coefficients for a typical  $IB$  response. The corresponding frequency spectra are shown

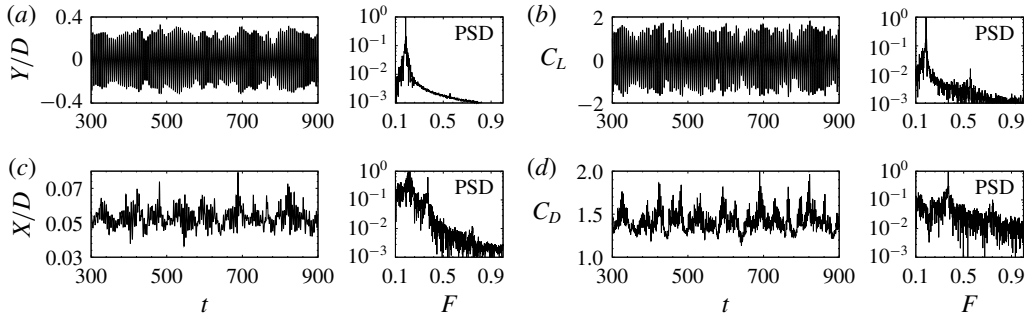


FIGURE 3. Flow past a freely vibrating cylinder for  $U^* = 4.7$  obtained via the increasing- $U^*$  approach: time history of (a) cylinder displacement in the transverse direction, (b) lift coefficient, (c) cylinder displacement in the streamwise direction and (d) drag coefficient. The corresponding frequency spectrum is shown alongside the time histories (PSD: power spectral density).

alongside the time histories. It is observed that the time signal for the transverse displacement and the lift coefficient is strongly modulated. This is in agreement with earlier experimental findings for  $Y$ -only oscillation (Khalak & Williamson 1999; Govardhan & Williamson 2000). The most dominant frequency in the two signals, identified as the frequency with the highest power in the corresponding frequency spectrum, is the same and equal to the vortex shedding frequency. The fluid–structure system, therefore, is in a state of lock-in/synchronization. We denote the common fluid–structure frequency as  $F_y$ . It is close to the natural frequency of the oscillator. For the flow past a non-oscillating cylinder, the frequency of the drag coefficient is twice the vortex shedding frequency. This is because of the spatio(transverse)-temporal symmetry of the flow past the cylinder (Blackburn, Marques & Lopez 2005). Since the VIV set-up in the present work is symmetric in the transverse direction, it is expected that the spatio-temporal symmetry of the flow will be preserved. Consequently, the frequency of the drag coefficient and the streamwise oscillation is expected to be  $2F_y$ . The frequency spectrum of  $C_D$  shows that the most dominant frequency is indeed  $2F_y$ . On the other hand, the frequency spectrum of the streamwise displacement shows two peaks. One at  $2F_y$ , and the other, which is the dominant of the two, at a frequency close to  $F_y$ . Hence, the most dominant frequency for streamwise and transverse oscillation is nearly the same. This is also evident in figure 4(a), which shows the streamwise and transverse displacements during three cycles of transverse oscillation of the cylinder. Further, as figure 3(c) shows, the motion of the cylinder in the streamwise direction is not symmetric about the mean streamwise position. These observations suggest that, compared to  $Y$ -only, there is a loss in the spatio-temporal symmetry of the  $XY$ -oscillating system. If the cylinder is constrained to move only in the streamwise direction, the frequency of streamwise oscillation is twice the vortex shedding frequency (Bourguet & Lo Jacono 2015), and the spatio-temporal symmetry is maintained. Therefore, the matching of the dominant frequency of streamwise and transverse oscillations on  $IB$  is attributed to the coupling between the motion in the two directions.

Williamson & Roshko (1988) studied forced transverse ( $Y$ -only) vibration of a circular cylinder in uniform flow and presented a map showing the co-relation between the vortex shedding pattern, and amplitude and frequency of cylinder oscillation.



### Intermittency in free vibration at subcritical $Re$

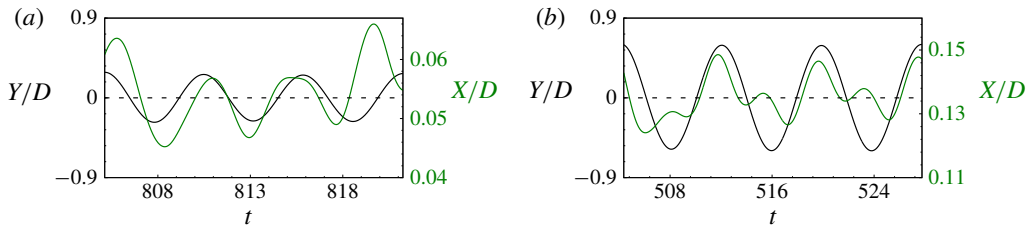


FIGURE 4. Flow past a freely vibrating cylinder: comparison of time histories of streamwise and transverse displacement of the cylinder for (a)  $U^* = 4.7$  and (b)  $U^* = 8.0$ .

The free-vibration data obtained from the present computations superimposed on the Williamson–Roshko map is shown in figure 1(b). In the original map, the frequency of cylinder oscillation is non-dimensionalized with the frequency of vortex shedding associated with a stationary cylinder. In the present work, the non-dimensionalization is carried out using the free-stream speed and diameter of the cylinder. It is observed that the data points for  $IB$  lie in the region of the  $2S$  mode on the Williamson–Roshko map. In the  $2S$  mode, two counter-rotating vortices of similar strength are shed per cycle of cylinder oscillation. We study the flow field to compare the results from the  $XY$  free oscillation with the Williamson–Roshko map. Figure 5(a) shows the span-averaged flow, in terms of spanwise vorticity, at three time instants during the motion of the cylinder from the highest to lowest transverse position. Also tracked in the figure is the release and convection of the counterclockwise (CCW) vortex from the lower surface of the cylinder. A similar activity, with respect to the clockwise (CW) vortex released from the upper surface, occurs in the next half of the cycle of cylinder motion. Hence, in each cycle of cylinder motion, one CCW and a CW vortex is shed in the wake. The vortex shedding mode, therefore, is  $2S$  and in excellent agreement with the Williamson–Roshko map.

#### 3.3. Intermittency between $UB^*$ and $LB^*$ : $4.7 \leq U^* \leq 5.8$

Figure 6 shows the time histories of the cylinder displacement and aerodynamic coefficients for three values of reduced speed:  $U^* = 4.7$  (obtained via the decreasing- $U^*$  approach) and 5.5 are, respectively, near the lower- and higher- $U^*$  end of the intermittent regime, while  $U^* = 5.1$  is in the middle of it. In  $Y$ -only oscillation, the  $UB$  and  $LB$  response for a given  $U^*$  differ in the amplitude of cylinder oscillation; compared to  $LB$ ,  $UB$  is associated with higher amplitude (Khalak & Williamson 1999; Govardhan & Williamson 2000; Williamson & Govardhan 2004). In  $XY$ -oscillation, though the  $UB^*$  and  $LB^*$  responses are generally well separated in terms of the transverse amplitude of the cylinder oscillation, they have similar values near the lower- $U^*$  end of the intermittent regime (inset of figure 1a). In this situation, intermittent behaviour is more apparent in the aerodynamic coefficients and streamwise response. Khalak & Williamson (1999) observed in their experiments that, during intermittency, the higher amplitude response ( $UB$ ) is associated with a higher value of mean drag. We use their finding to separate the  $UB^*$  and  $LB^*$  responses in the time histories for  $U^* = 4.7$ . To this end, the average value of drag coefficient over each cycle of cylinder oscillation in the transverse direction ( $\overline{C_D}$ ) is calculated. Its variation with time is shown by the thick red line atop the time history of  $C_D$  in figure 6(c). The intermittent switching between  $UB^*$  and  $LB^*$  is

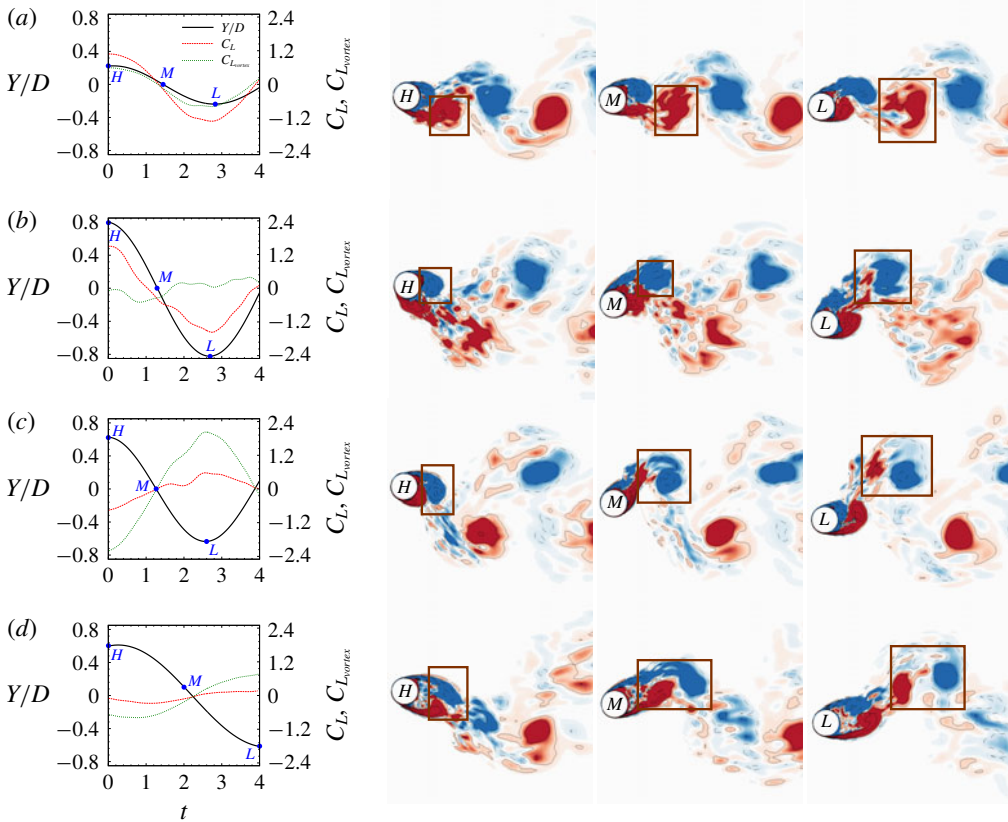


FIGURE 5. Flow past a freely vibrating cylinder for (a)  $U^* = 4.7$  (*IB* response), (b)  $U^* = 5.3$  (*UB\** response during intermittency), (c)  $U^* = 5.3$  (*LB\** response during intermittency) and (d)  $U^* = 8.0$  (*LB* response). The line plot shows the time histories of the cylinder transverse displacement,  $C_L$  and  $C_{L_{vortex}}$  as the cylinder descends from its highest to lowest transverse location, while the remaining columns show the instantaneous span-averaged spanwise vorticity near the highest (*H*), mean (*M*) and lowest (*L*) transverse position of the cylinder. These locations as well as the corresponding time instants are marked on the curve for transverse displacement in the line plot. For each case, a certain flow structure is tracked via a rectangular frame.

evident in the relatively large decrease/increase in  $\widetilde{C}_D$ . The time intervals during which the response is associated with *UB\** is shaded in figure 6. It is observed that the amplitude of the streamwise displacement and cycle-averaged mean value of the streamwise displacement is higher for *UB\** than *LB\**. For  $U^* = 4.7$ , the amplitude of the lift coefficient for *UB\** is found to be lower than for *LB\**.

With an increase in  $U^*$ , the difference in the amplitude of the transverse oscillation between *UB\** and *LB\** increases, thereby making the switching apparent in the transverse response of the cylinder (see  $U^* = 5.1$  and  $5.5$  in figure 6*a*). The streamwise amplitude of the cylinder oscillation as well as  $\widetilde{C}_D$  for *UB\** is higher than that for *LB\**. This is in line with the method adopted by us for separating the *UB\** and *LB\** responses for  $U^* = 4.7$ . For  $U^* = 5.1$  and  $5.5$ , the amplitude of  $C_L$  associated with *UB\** is higher than for *LB\**.



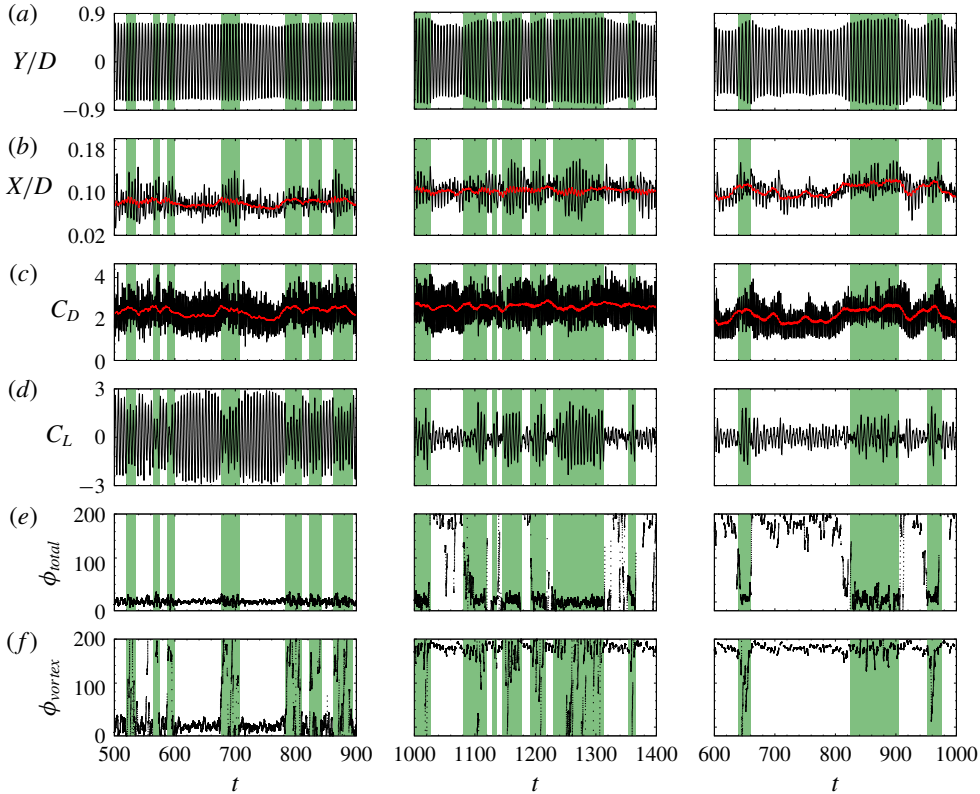


FIGURE 6. Flow past a freely vibrating cylinder in the intermittent regime: time histories of (a) transverse cylinder displacement, (b) streamwise cylinder displacement, (c) drag coefficient, (d) lift coefficient, (e)  $\phi_{total}$  and (f)  $\phi_{vortex}$ . The variation of cycle-averaged value for  $X/D$  and  $C_D$  is shown using a thick red line in (b) and (c), respectively. The time histories from left to right are for  $U^* = 4.7$  (decreasing  $U^*$ ),  $U^* = 5.1$  and  $U^* = 5.5$ , respectively. In each subfigure, the  $UB^*$  response is shaded in green.

Near the higher- $U^*$  end of intermittent regime, the system exhibits the  $LB^*$  response for most of the time ( $U^* = 5.5$  in figure 6), and the time interval between the successive appearance of the  $UB^*$  response becomes relatively large. It is, therefore, plausible that intermittent switching between  $UB^*$  and  $LB^*$  exists beyond  $U^* = 5.8$  as well. However, due to constraints of the computational resources available to us at present, the computation could not be carried out for long enough to ascertain intermittent behaviour of the system beyond  $U^* = 5.8$ .

Figure 7 shows the variation of intermittency factor ( $IF$ ) with  $U^*$  in the intermittent flow regime.  $IF$  is defined as the fraction of time during which the response of the fluid–structure system is associated with the  $UB^*$  response. It is observed that for  $U^* \lesssim 5.3$ , the system has a preference for the  $UB^*$  response, as is evident from the value of  $IF$  being greater than 0.5. On the other hand, for  $U^* \gtrsim 5.3$ , the system is biased towards the  $LB^*$  response. The variation of  $IF$  with  $U^*$  is non-monotonic;  $IF$  increases with  $U^*$  up to  $U^* = 5.1$ , and thereafter decreases. This is in line with the time histories shown in figure 6, where the fraction of the shaded region (that corresponds to  $UB^*$  response) in the time history for  $U^* = 5.1$  is higher than that for  $U^* = 4.7$  and 5.5.

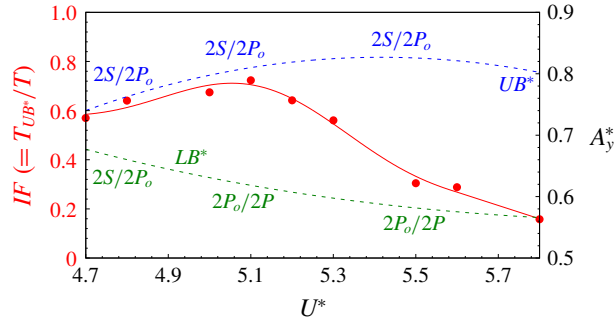


FIGURE 7. Flow past a freely vibrating cylinder: variation of intermittency factor ( $IF$ ) with reduced speed in the intermittent flow regime shown as filled (red) circles. The least-squares curve fit for the  $IF$  data points is shown using a solid (red) line. Also shown using broken lines is the amplitude response curve for  $UB^*$  (blue) and  $LB^*$  (green) from figure 1(a). The modes of vortex shedding at various  $U^*$  while the flow switches between  $LB^*$  and  $UB^*$  are marked on the response curves.

The Williamson–Roshko map shown in figure 1(b) predicts three modes of vortex shedding in the intermittent regime:  $2S$ ,  $2P$  and  $2P_o$ . In the  $2P$  and  $2P_o$  mode of vortex shedding, two pairs of counter-rotating vortices are shed in one cycle of transverse oscillation of the cylinder. While the strength of the counter-rotating vortices in each pair is equal in the  $2P$  mode, they are different in the  $2P_o$  mode. According to the map, the  $UB^*$  response can be associated with either the  $2S$  or  $2P_o$  mode, while the  $LB^*$  response can be associated with any of the three modes. During intermittency, the flow switches between different modes of vortex shedding. Figure 5(b) shows the spanwise vorticity for  $U^* = 5.3$  ( $UB^*$ ) at different time instants during the motion of the cylinder from the highest to the lowest transverse position. The same for  $U^* = 5.3$  ( $LB^*$ ) is shown in figure 5(c). In the  $UB^*$  response, one CW (blue) vortex is shed in the wake as the cylinder reaches the lowest position. In addition to the CW vortex, we also observe a relatively smaller patch of positive vorticity (red) getting detached from the cylinder surface (see the region within the rectangle in the  $L$  position of figure 5b). For  $U^* = 5.3$  ( $LB^*$ ), a pair of counter-rotating vortices is shed when the cylinder has reached the lowest position (see the region within the rectangle in the  $L$  position of figure 5c). The strength of the CW vortex (blue) in the pair appears to be higher than that of the CCW vortex (red). This mode of vortex shedding is reminiscent of the  $2P_o$  mode. The relative strength of the weaker vortex varies from one cycle of the cylinder oscillation to the other. In some situations, the weaker vortex is imperceptible, and the vortex shedding pattern resembles the  $2S$  mode. It is, therefore, difficult to associate a definite vortex shedding pattern to either the  $UB^*$  or the  $LB^*$  response from flow visualization. We circumvent this difficulty by utilizing the co-relation between the mode of vortex shedding and the phase difference between the transverse displacement of the cylinder and lift coefficient that has been established in earlier VIV studies. In general, the lift coefficient can be split in two parts:  $C_{L_{vortex}}$  and  $C_{L_{potential}}$ . The former is attributed to vortex force and the latter is associated with the potential force (Lighthill 1986; Govardhan & Williamson 2000). We denote the phase difference between  $Y/D$  and total  $C_L$  by  $\phi_{total}$  and that between  $Y/D$  and  $C_{L_{vortex}}$  by  $\phi_{vortex}$ . The following co-relations have been reported between the vortex shedding modes and the two phase angles (Govardhan & Williamson 2000;

Navrose & Mittal 2013; Zhao *et al.* 2014) –

$$\left. \begin{aligned} 2S: \phi_{total} \sim 0^\circ, \quad \phi_{vortex} \sim 0^\circ, \\ 2P_o: \phi_{total} \sim 0^\circ, \quad \phi_{vortex} \sim 180^\circ, \\ 2P: \phi_{total} \sim 180^\circ, \quad \phi_{vortex} \sim 180^\circ. \end{aligned} \right\} \quad (3.1)$$

To demonstrate the co-relation, we consider the  $U^* = 4.7$  flow (obtained via the increasing- $U^*$  approach). The response is on  $IB$  and the mode of vortex shedding in  $2S$  (figure 5a). In this situation, both  $\phi_{total}$  and  $\phi_{vortex}$  are expected to be close to zero. This indeed is the case, as evident from the line plot in figure 5(a), which shows the time history of  $Y/D$ ,  $C_L$  and  $C_{L_{vortex}}$  over a half-cycle of cylinder transverse oscillation.

We explore the co-relation between the two phase angles and mode of vortex shedding for three values of  $U^*$  ( $= 4.7, 5.1$  and  $5.5$ ) in the intermittent regime. In the intermittent regime, since the vortex shedding flips between different modes, we cannot use a plot similar to figure 5(a) to estimate  $\phi_{total}$  and  $\phi_{vortex}$ . Instead, we use the Hilbert transform to obtain the time variation of  $\phi_{total}$  and  $\phi_{vortex}$ . The method is the same as that used by Zhao *et al.* (2014) for  $Y$ -only oscillation. In the first step, the Hilbert transform of the time signals of  $C_L$ ,  $C_{L_{vortex}}$  and  $Y/D$  is carried out to estimate the time variation of the phase associated with the three signals. Thereafter, at each time instant, the phase of  $C_L$  and  $C_{L_{vortex}}$  is subtracted from the phase of  $Y/D$  to obtain instantaneous values of  $\phi_{total}$  and  $\phi_{vortex}$ , respectively. Figures 6(e) and 6(f) shows, respectively, the variation of  $\phi_{total}$  and  $\phi_{vortex}$  with time for  $U^* = 4.7$  (decreasing  $U^*$ ),  $5.1$  and  $5.5$ . For  $U^* = 4.7$ ,  $\phi_{total}$  is close to zero at all times. On the other hand,  $\phi_{vortex}$  is mostly close to zero for the  $LB^*$  response (occasionally, the value of  $\phi_{vortex}$  for the  $LB^*$  response jumps close to  $180^\circ$ , as is evident in figure 6f at  $t \sim 550$ ), and is either close to zero or  $180^\circ$  for the  $UB^*$  response. Therefore, based on the aforementioned co-relations, the mode of vortex shedding for the  $U^* = 4.7$   $LB^*$  response is largely  $2S$ , with the occasional appearance of the  $2P_o$  mode, and it regularly switches between the  $2S$  and  $2P_o$  modes for the  $UB^*$  response. A similar mix of the  $2S$  and  $2P_o$  modes is observed for the  $UB^*$  response of the  $U^* = 5.1$  flow. The  $LB^*$  response for the  $U^* = 5.1$  flow is found to be associated with either the  $2P_o$  or  $2P$  mode. For  $U^* = 5.5$ , the mode of vortex shedding for the  $LB^*$  and the  $UB^*$  response is largely  $2P$  and  $2P_o$ , respectively, with occasional signatures of the  $2P_o$  mode in the former response and the  $2S$  mode in the latter response.

The occurrence of different modes of vortex shedding during the intermittent regime in  $XY$ -oscillation has been reported for  $Y$ -only vibration as well (Zhao *et al.* 2014). Zhao *et al.* (2014) used the maximum amplitude of transverse oscillation in the entire time history to plot the response curve in the intermittent regime, and referred to it as the  $UB$  response. They found that near the lower- $U^*$  end of the intermittent regime, the flow switches between the  $2S$  and  $2P_o$  modes of vortex shedding, while it switches between the  $2P_o$  and  $2P$  modes near the higher- $U^*$  end of the intermittent regime. For the  $XY$ -oscillation, we observe that for the entire  $UB^*$ , the vortex shedding mode switches between  $2S$  and  $2P_o$ . The system appears to have a higher preference for the  $2P_o$  mode than the  $2S$  mode, as is evident from the combination of  $\phi_{total}$  and  $\phi_{vortex}$  during the  $UB^*$  response for  $U^* = 4.7, 5.1$  and  $5.5$  (shaded part of figure 6e,f). For the  $LB^*$  response, the results of the  $XY$ -oscillation suggest that the mode of vortex shedding could be  $2S, 2P_o$  and  $2P$ . Near the lower- $U^*$  end of the intermittent regime, the mode of vortex shedding for  $LB^*$  is mostly  $2S$ . In the middle and higher- $U^*$  end of the intermittent regime, the wake is a mix of the  $2P_o$  and  $2P$  modes. Therefore, in

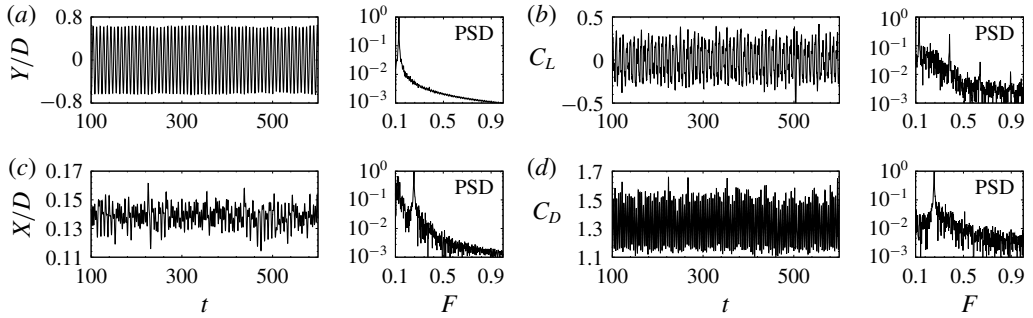


FIGURE 8. Flow past a freely vibrating cylinder for  $U^* = 8.0$ : time history of (a) cylinder displacement in the transverse direction, (b) lift coefficient, (c) cylinder displacement in the in-line direction and (d) drag coefficient. The corresponding frequency spectrum is shown alongside the time histories (PSD: power spectral density).

both  $XY$ - and  $Y$ -only oscillation, the intermittent regime consists of a mixture of  $2S$ ,  $2P_o$  and  $2P$  modes of vortex shedding. The present study further brings out the flow characteristics during intermittency. The modes of vortex shedding, during intermittent switch between the  $LB^*$  and  $UB^*$  response, at various  $U^*$  are marked in figure 7.

### 3.4. Lower branch: $5.9 \leq U^* \leq 10.4$

Figure 8 shows the time histories of cylinder displacement and aerodynamic coefficients for  $U^* = 8.0$ . The corresponding frequency spectrum is shown alongside the time histories. The most dominant frequency for the transverse oscillation and the lift coefficient is the same. As earlier, we refer to the common fluid–structure frequency by  $F_y$ . Compared to  $IB$  and intermittent regime, the level of fluctuation in the lift coefficient for  $LB$  is lower. The most dominant frequency for the streamwise oscillation and the drag coefficient is the same, and is equal to  $2F_y$ . Similar to the  $IB$  response, the frequency spectrum of the streamwise response for  $LB$  shows that the  $F_y$  component is comparable in strength to the most dominant frequency. Figure 4(b) shows a close-up view of the time histories of the transverse and streamwise oscillations. Within one cycle of transverse oscillation, two peaks, one large and the other small, are observed in the streamwise response. The successive peaks occur at a frequency of  $2F_y$ , while the pattern of a large peak followed by a small peak occurs at frequency  $F_y$ .

Figure 5(d) shows the spanwise vorticity for  $LB$ . Compared to  $IB$  and the intermittent regime, the transverse width of the wake for  $LB$  is larger. Two pairs of counter-rotating vortices are shed in one cycle of cylinder transverse oscillation. The two vortices in each vortex pair are of equal strength. Further, both  $\phi_{total}$  and  $\phi_{vortex}$  are close to  $180^\circ$ , as seen from the line plot in figure 5(d). The mode of vortex shedding, therefore, is  $2P$ . This matches with the results of  $Y$ -only oscillation (Govardhan & Williamson 2000; Zhao *et al.* 2014).

## 4. Conclusions

A two-degree-of-freedom VIV system has been investigated via numerical simulation in the subcritical- $Re$  flow regime ( $1500 \lesssim Re \lesssim 9000$ ) for moderate mass ratio ( $m^* = 10$ ). The range of the lock-in regime spans  $IB$ ,  $LB$  and a regime where

intermittent switching occurs between a high- ( $UB^*$ ) and a low-amplitude response ( $LB^*$ ). The mode of vortex shedding for the  $UB^*$  response is found to be a mix of  $2S$  or  $2P_o$ , while it can be either  $2S$ ,  $2P_o$  or  $2P$  for the  $LB^*$  response. It is observed that while the transverse force and oscillation are synchronized with respect to the most dominant frequency in the corresponding frequency spectra for the entire lock-in regime, it is not the same for in-line force and oscillation. For example, for the  $IB$  response, the most dominant frequency in the streamwise and transverse oscillations is the same, and is half the value of the most dominant frequency in  $C_D$ . On the other hand, for the  $LB$  response, the most dominant frequency in the streamwise oscillation and  $C_D$  is the same, and is twice that of transverse oscillation. In  $XY$ -oscillation, the system exhibits hysteresis near the higher- $U^*$  end of the lock-in regime that has not been reported in earlier experimental studies on  $Y$ -only oscillation. The present work shows that the transition between various branches of cylinder response and desynchronization regimes is sensitive to streamwise oscillation even for systems with moderate mass ratios.

## Acknowledgements

The authors would like to thank Mr S. Kumar for his assistance during compilation of the data. We are grateful to Dr S. Behara, Mr A. Desai, Mr M. Furquan, Mr T. R. Sahu and Mr G. Chopra for their help with large-scale computations and flow visualization. We acknowledge the use of computational resources at the High Performance Computing facility, Computer Center, Indian Institute of Technology Kanpur that has been set up with assistance from the Department of Science and Technology (DST), India. We would also like to thank the anonymous reviewers for their feedback and insightful suggestions.

## References

- BEARMAN, P. W. 2011 Circular cylinder wakes and vortex-induced vibrations. *J. Fluids Struct.* **27**, 648–658.
- BLACKBURN, H. M., MARQUES, F. & LOPEZ, J. M. 2005 Symmetry breaking of two-dimensional time-periodic wakes. *J. Fluid Mech.* **522**, 395–411.
- BOURGUET, R. & LO JACONO, D. 2015 In-line flow-induced vibrations of a rotating cylinder. *J. Fluid Mech.* **781**, 127–165.
- GOVARDHAN, R. & WILLIAMSON, C. H. K. 2000 Modes of vortex formation and frequency response of a freely vibrating cylinder. *J. Fluid Mech.* **420**, 85–130.
- GOVARDHAN, R. & WILLIAMSON, C. H. K. 2002 Resonance forever: existence of a critical mass and an infinite regime of resonance in vortex-induced vibration. *J. Fluid Mech.* **473**, 147–166.
- GOVARDHAN, R. & WILLIAMSON, C. H. K. 2006 Defining the modified Griffin plot in vortex-induced vibration: revealing the effect of Reynolds number using controlled damping. *J. Fluid Mech.* **561**, 147–180.
- JAUVTIS, N. & WILLIAMSON, C. H. K. 2004 The effect of two degrees of freedom on vortex-induced vibration at low mass and damping. *J. Fluid Mech.* **509**, 23–62.
- KHALAK, A. & WILLIAMSON, C. H. K. 1999 Motions, forces and mode transitions in vortex-induced vibrations at low mass-damping. *J. Fluids Struct.* **13** (7), 813–851.
- LIGHTHILL, J. 1986 Wave loading on offshore structures. *J. Fluid Mech.* **173**, 667–681.
- NAVROSE & MITTAL, S. 2013 Free vibrations of a cylinder: 3-D computations at  $Re = 1000$ . *J. Fluids Struct.* **41**, 109–118.
- NAVROSE & MITTAL, S. 2017 The critical mass phenomenon in vortex-induced vibration at low  $Re$ . *J. Fluid Mech.* **820**, 159–186.
- NAVROSE, YOGESWARAN, V., SEN, S. & MITTAL, S. 2014 Free vibrations of an elliptic cylinder at low Reynolds numbers. *J. Fluids Struct.* **51**, 55–67.

- PRASANTH, T. K. & MITTAL, S. 2008 Vortex-induced vibrations of a circular cylinder at low Reynolds numbers. *J. Fluid Mech.* **594**, 463–491.
- RYAN, K. C., THOMPSON, M. C. & HOURIGAN, K. 2005 Variation in the critical mass ratio of a freely oscillating cylinder as a function of Reynolds number. *Phys. Fluids* **17** (3), 038106.
- SARPKAYA, T. 2004 A critical review of the intrinsic nature of vortex-induced vibrations. *J. Fluids Struct.* **19**, 389–447.
- SINGH, S. P. & MITTAL, S. 2005 Vortex-induced oscillations at low Reynolds numbers: hysteresis and vortex-shedding modes. *J. Fluids Struct.* **20** (8), 1085–1104.
- WILLIAMSON, C. H. K. & GOVARDHAN, R. 2004 Vortex-induced vibrations. *Annu. Rev. Fluid Mech.* **36**, 413–455.
- WILLIAMSON, C. H. K. & ROSHKO, A. 1988 Vortex formation in the wake of an oscillating cylinder. *J. Fluids Struct.* **2** (4), 355–381.
- ZHAO, J., LEONTINI, J. S., LO JACONO, D. & SHERIDAN, J. 2014 Chaotic vortex induced vibrations. *Phys. Fluids* **26** (12), 121702.